



Electrochemical behaviour investigation of two low activation austenitic stainless steels in an acidic solution

A. Fattah-alhosseini^{1,*}, F. Shirsalimi², M. Yousefi³, A. Abedi²

¹ Faculty of Engineering, Bu-Ali Sina University, Hamedan 65178-38695, Iran

² Department of Materials Engineering, Faculty of Mechanical Engineering, Shahid Rajaei Teacher Training University, Tehran 16785-136, Iran

³ Energy and Mechanical Engineering Department, Abbaspour College of Engineering, Shahid Beheshti University, P.O. Box.16765-1719, Tehran, Iran

Received 23 January 2014; Revised 8 October 2014; Accepted 8 October 2014.

*Corresponding Author. E-mail: a.fattah@basu.ac.ir; Tel: (+988118292505)

Abstract

In this paper, two stainless steels have been developed successfully. The physical metallurgy of these stainless steels was studied by optical microscope, and X-ray diffraction (XRD) patterns. Metallography and XRD results have shown that the matrix of these stainless steels is a single γ -phase structure. Also, electrochemical behaviour of two fabricated stainless steels in 0.5M H₂SO₄ solution was evaluated by open-circuit potential, potentiodynamic polarization, and Mott–Schottky analysis. The potentiodynamic polarisation curves suggested that two fabricated stainless steels showed passive behaviour in 0.5M H₂SO₄ solution. Mott–Schottky analysis revealed that passive films behave as n-type and p-type semiconductors at potentials below and above the flat band potential, respectively. Also based on the Mott–Schottky analysis, it was shown that donor and acceptor densities are in the order of 10²¹ cm⁻³ and are comparable for other austenitic stainless steels in acidic environments.

Keywords: Stainless steel; Polarization; XRD; Mott–Schottky.

Introduction

Fe-Cr-Mn-C stainless steels (low activation austenitic stainless steels) are candidate materials for structural components of fusion reactors because of their low induced long-term radioactivity compared to that of typical Fe-Cr-Ni austenitic stainless steels [1-3]. These stainless steels are possible alternatives to Fe-Cr-Ni-based austenitic stainless steels, on the basis of substitution of the strategic element Ni by the more plentiful and cheaper metal Mn [4-6].

Other main advantages of Fe-Cr-Mn-C stainless steels can be found in their applications in wear-resistant and pitting-resistant steel products. These stainless steels have also been successfully applied in the superconductor industries. This is mainly because of their higher strengths in cryogenic environments [7-9].

Various types of low activation austenitic stainless steels have been developed based on Mn–Cr non-magnetic steels [10-12]. Harries et al. [13] and Kohyama et al. [14] have reported that the phase and properties of Mn–Cr steels are unstable under irradiation at high temperature. Although the applicability of the steels to fusion reactor components may be limited due to such characteristics, further investigation has been conducted to optimize their properties and minimize the effects of radiation damage. Shamardin et al. [15] have investigated various types of low activation austenitic stainless steel based on Mn–Cr non-magnetic steels. However, those alloys still have small amounts of Ni, Co, Mo, etc. which cause problems of long-life activation.

In the present study, research has been conducted firstly to eliminate such undesirable elements and produce lower activation austenitic stainless steels that can be manufactured along usual industrial production lines. Also, low activation austenitic stainless steels frequently come in contact with acids during the process like cleaning, and pickling. Therefore, studying the corrosion behaviour of these stainless steels in the acidic medium is of prime importance. Therefore, research has also been focused on the corrosion behaviour of Low activation austenitic stainless steels in 0.5M H₂SO₄ solution.

2. Materials and methods

Two austenitic stainless steels listed in Table 1 were fabricated by a vacuum high-frequency induction furnace which was used to cast a single ingot for each steels.

Table 1: Chemical compositions of two fabricated austenitic stainless steels.

Elements	C	Mn	Cr	Si	P	S	V	Ti	Fe
Stainless Steel 1	0.233	18.54	12.66	0.0676	0.0065	0.0087	0.0721	0.0003	Bal.
Stainless Steel 2	0.294	18.26	10.32	0.103	0.0055	0.0077	0.0501	0.0020	Bal.

To prepare sheets from these stainless steels, hot rolling was carried out on 40 mm thick ingots. Initially the stainless steels were heated to 1200°C for 120 min. afterward the thickness was reduced to 30 and then 22 mm. Subsequently the sheets were heated to 1100°C for 10 min. and a further reduction in thickness to 18 and finally 10 mm was applied on the sheets. In order to achieve a homogenous structure annealing was carried out at 1050°C for 10 minutes, and finally the sheets were quenched in water.

To examine the acquired structure an optical microscope of the type Lecia was used. The samples were polished and etched in a solution containing 200 ml HCl + 1000 ml water + 100ml solution containing 0.5-1 gr K₂S₂O₅. Also XRD was used for phase evaluations using a Philips PW-1800 diffractometer, with a Cu K_α radiation source.

For electrochemical measurements, samples were cut from the plates and polished mechanically by abrading with wet emery paper up to 2000 grit on all sides and then were embedded in cold curing epoxy resin. Prior to all measurements, working electrodes were degreased with acetone, rinsed with distilled water and dried with a stream of air.

Electrochemical measurements were performed in a conventional three-electrode cell under aerated conditions. The counter electrode was a Pt plate, while the reference electrode was Ag/AgCl saturated in KCl. Electrochemical measurements were obtained by using a Autolab potentiostat/galvanostat system. Prior to all electrochemical measurements, working electrodes immersed at open circuit potential (OCP) for 0.5 h to form a steady-state passive film.

Potentiodynamic polarization curves were measured potentiodynamically at a scan rate of 1 mV/s starting from -0.25 V_{Ag/AgCl} (vs. E_{corr}) to 2.0 V_{Ag/AgCl}. Mott-Schottky analysis were carried out on passive films at a frequency of 1 kHz using a 10 mV ac signal, and a step rate of 25 mV in the cathodic direction.

3. Results and discussion

3.1. Development of low activation austenitic stainless steels

Mn is an important element to stabilize the austenite structure. However, an excess amount of Mn accelerates the production of intermetallic compounds and lowers ductility and corrosion resistance. Therefore, Mn was limited between 15% and 35%. Otherwise, a Cr content of more than 11% improves corrosion resistance. On the other hand, an excess amount of Cr destabilizes the austenite structure; therefore, the Cr content was limited in the range of 11% to 20%. Si is an effective deoxidizing element. An excess amount of Si, however, leads to the destabilization of the austenite structure. As such, the Si content was limited to 1.0%. Reduction of strength caused by the decreased amounts of C and N can be compensated for by adding V, which is intended to precipitate carbide and/or nitride. However, since an excess of V reduces weldability, V was restricted to 0.3%. Adjustment of alloying elements was conducted to obtain a single austenitic phase according to the constitution of austenitic stainless steels, which was based on the constitution diagrams of Schaeffler. Development of the Mn-Cr based stainless steels was done by considering the above factors [16].

The Schaeffler diagram shown in Fig. 1 is one of the means of determining the stability of austenite and other phases in the matrix of stainless steels. For the Schaeffler diagram, the nickel and chromium equivalents were calculated according to the following relationships [17, 18]:

$$Ni_e = (Ni) + (Co) + 0.5 (Mn) + 0.3 (Cu) + 25 (N) + 30 (C) \quad (1)$$

$$Cr_e = (Cr) + 2 (Si) + 1.5 (Mo) + 5 (V) + 5.5 (Al) + 1.75 (Nb) + 1.5 (Ti) + 0.75 (W) \quad (2)$$

where the concentrations of the respective elements given in parentheses are in weight percent.

Klueh et al. [17] illustrated that Schaeffler diagram is not able to predict the amount of phases in steels containing high amounts of Mn and needs some corrections. This led to a new Schaeffler diagram for steels containing high amounts of Cr and Mn (maximum 40 wt.%Mn) and is shown in Fig. 2. Table 2 shows the calculated Chromium and Nickel equivalents using relations 1 and 2 for two types of austenitic stainless steels. It is apparent that using corrected Schaeffler diagram, the matrix of two stainless steels is single phase austenite.

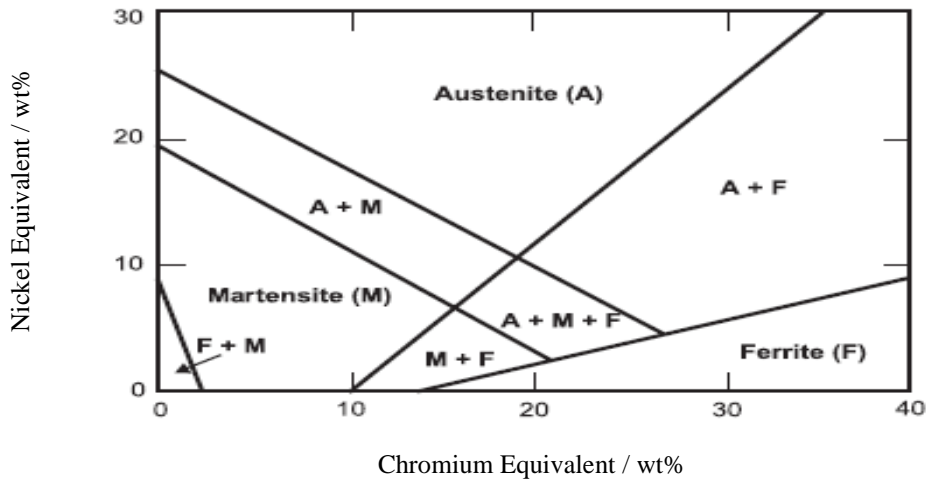


Figure 1: The Schaeffler diagram [17].

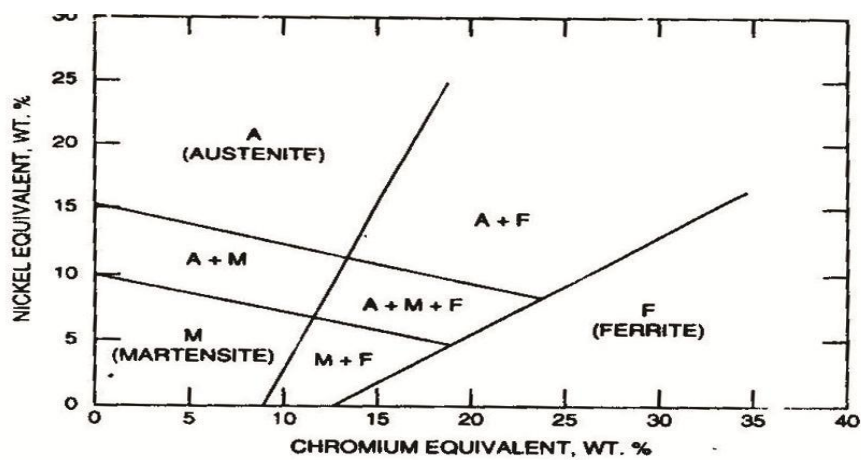


Fig. 2: The corrected Schaeffler diagram for steels containing high amounts of Cr and Mn (maximum 40 wt.% Mn) [17].

Table 2: The calculated Cr and Ni equivalents for two fabricated stainless steels.

	<i>Stainless steel 1</i>	<i>Stainless steel 2</i>
Cr Equivalent / wt%	12.81	10.53
Ni Equivalent/ wt%	16.26	17.95

3.2. Microstructure behaviour

The optical micrographs of the surfaces for two types of austenitic stainless steels are given in Fig. 3. It is illustrated that the structures of two austenitic stainless steels are fully austenite and contain a very large number of twins which is characteristic appearance of these types of steels.

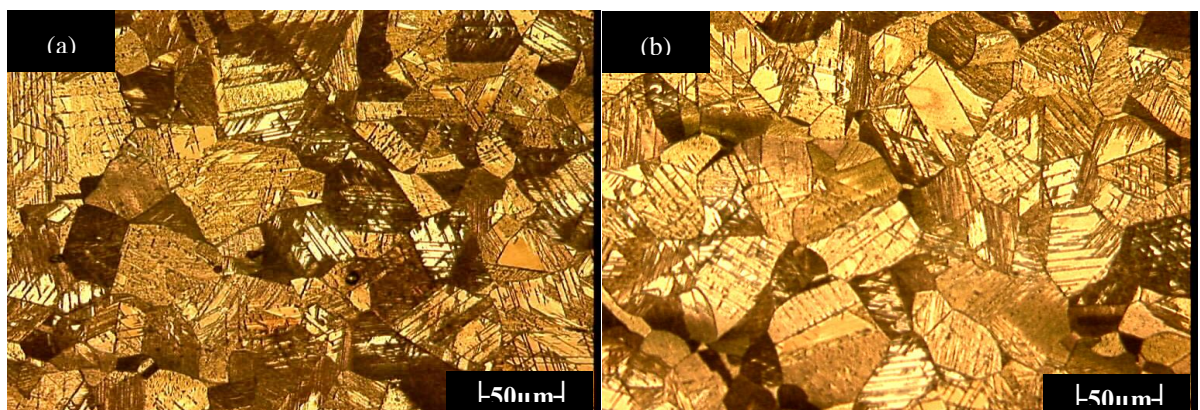


Figure 3: Optical micrographs of two fabricated: (a) stainless steel 1, and (b) stainless steel 2.

Fig. 4 shows the X-ray diffraction patterns of two types of austenitic stainless steels which show the XRD patterns of single austenite peak.

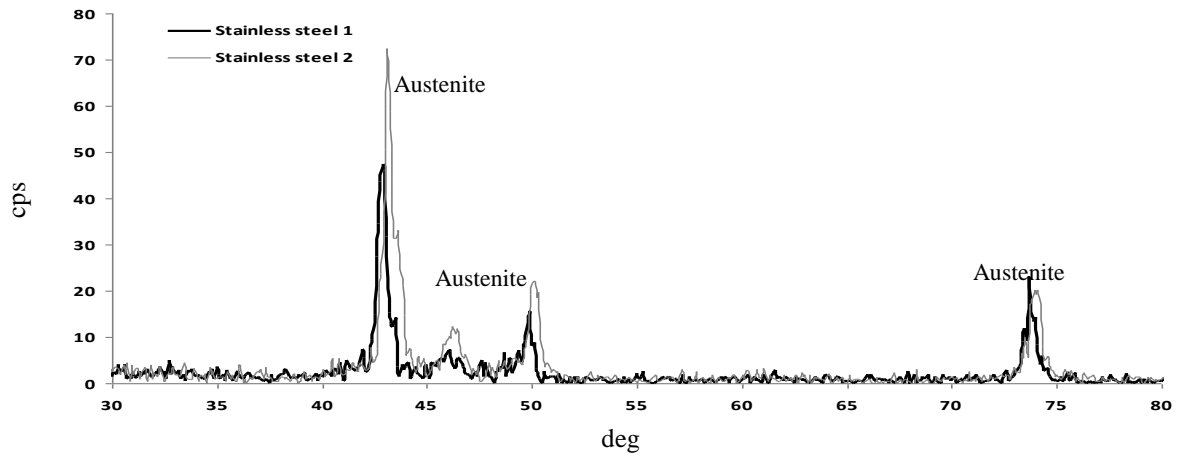


Figure 4: XRD patterns of two fabricated stainless steel.

3.3. Corrosion behaviour

In Fig. 5 changes on OCP of two austenitic stainless steels in 0.5M H₂SO₄ solution is shown. At the start of immersion a reduction of the potential in two austenitic stainless steels immediately show the dissolution of oxide layer of the surface in an acidic environment. However, as time passes, the open circuit potentials tend towards positive amount. This trend is also reported for austenitic stainless steels in an acidic environment [19] which is indicative of the formation of growing layer and its role in increasing protectivity with time. Fig. 5 also indicates that after 1800 s a complete stable condition is achieved and electrochemical tests are possible.

Fig. 6 shows the potentiodynamic polarization curves of two austenitic stainless steels in 0.5M H₂SO₄ solution. For two curves, it is observed that before the electrode surface is transferred to a passive state an active current peak occurs, which could be related to the oxidation of Fe²⁺ to Fe³⁺ ions in the passive film [20, 21].

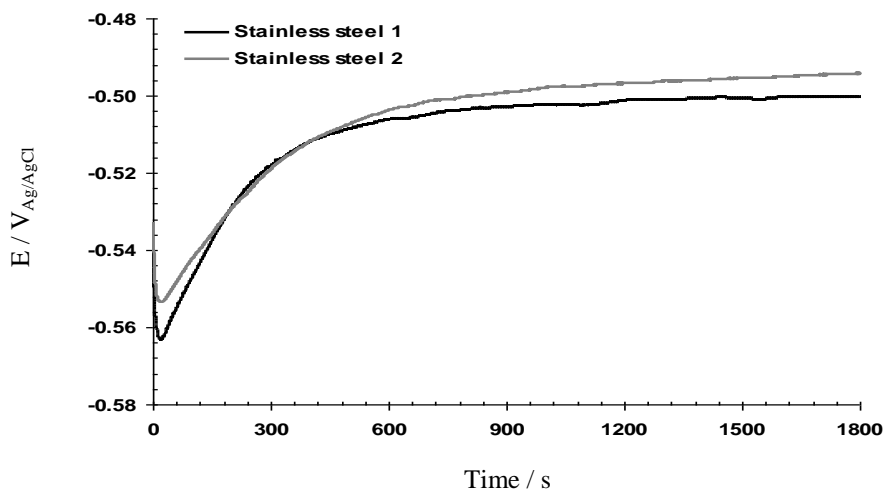


Figure 5: OCP plots of two fabricated stainless steels in 0.5M H₂SO₄ solution.

3.4. Mott-Schottky analysis

The outer layer of passive films contains the space charge layer and sustains a potential drop across the film. The charge distribution at the semiconductor/solution is usually determined based on Mott-Schottky relationship by measuring electrode capacitance C, as a function of electrode potential (E) [22-25]:

$$\frac{1}{C^2} = \frac{2}{\epsilon_0 e N_D} \left(E - E_{FB} - \frac{kT}{e} \right) \quad \text{for n-type semiconductor} \quad (3)$$

$$\frac{1}{C^2} = -\frac{2}{\epsilon_0 e N_A} \left(E - E_{FB} - \frac{kT}{e} \right) \quad \text{for p-type semiconductor} \quad (4)$$

where e is the electron charge (-1.602×10^{-19} C), N_D is the donor density for n-type semiconductor (cm^{-3}), N_A is the acceptor density for p-type semiconductor (cm^{-3}), ϵ is the dielectric constant of the passive film (usually taken as 15.6), ϵ_0 is the vacuum permittivity (8.854×10^{-14} F cm^{-1}), k is the Boltzmann constant (1.38×10^{-23} J K^{-1}), T is the absolute temperature and E_{FB} is the flat band potential [22-25].

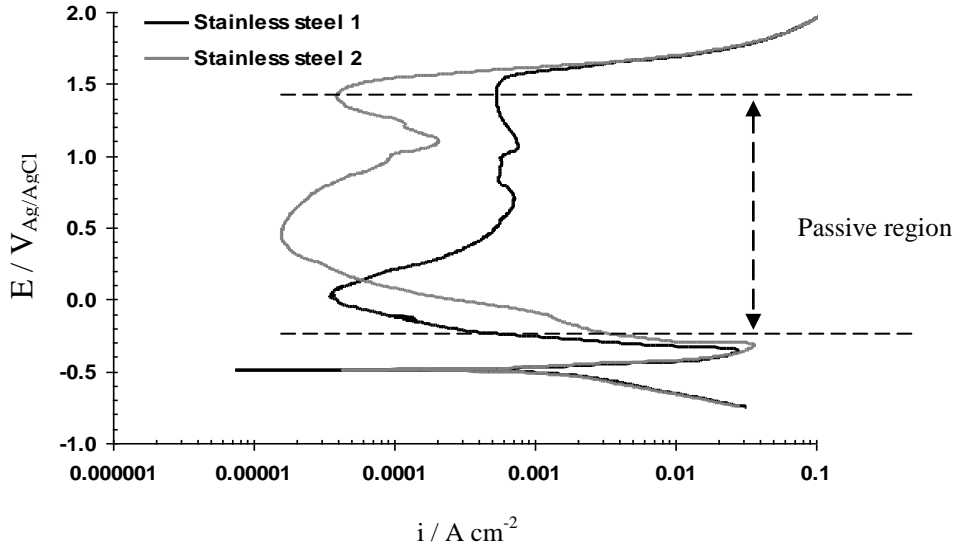


Figure 6: Potentiodynamic polarization plots of two fabricated stainless steels in 0.5M H_2SO_4 solution.

Fig. 7 shows the Mott-Schottky plots of two austenitic stainless steels in 0.5M H_2SO_4 solution. Clearly, all plots show four regions in which a linear relationship between C^{-2} and E could be observed from them. The negative slopes in regions I and III are attributed to p-type behaviour. Regions I and IV present positive slopes, which depicts an n-type semiconducting behaviour.

Fig. 7 shows the passive films formed on these stainless steels behave as both n-type and p-type semiconductors. This behaviour implies that the passive films have a duplex structure. Early studies of the bipolar duplex structures of passive films on stainless steels was done by Sato [26], and followed by Ferreira et al [27], and Oguzie et al. [28]. It has been well established that the inner part of the passive film, which has a p-type behaviour, consists mainly of Cr oxides, while the outer region, with an n-type behaviour, predominantly consists of Fe oxides [29].

According to Eq. (3) and (4), donor and acceptor densities are determined by positive and negative slopes in regions II and III. Table 3 shows the calculated donor and acceptor densities for two austenitic stainless steels in 0.5M H_2SO_4 solution. The orders of magnitude are around 10^{21} cm^{-3} and are comparable for other austenitic stainless steels in acidic environments [30, 31].

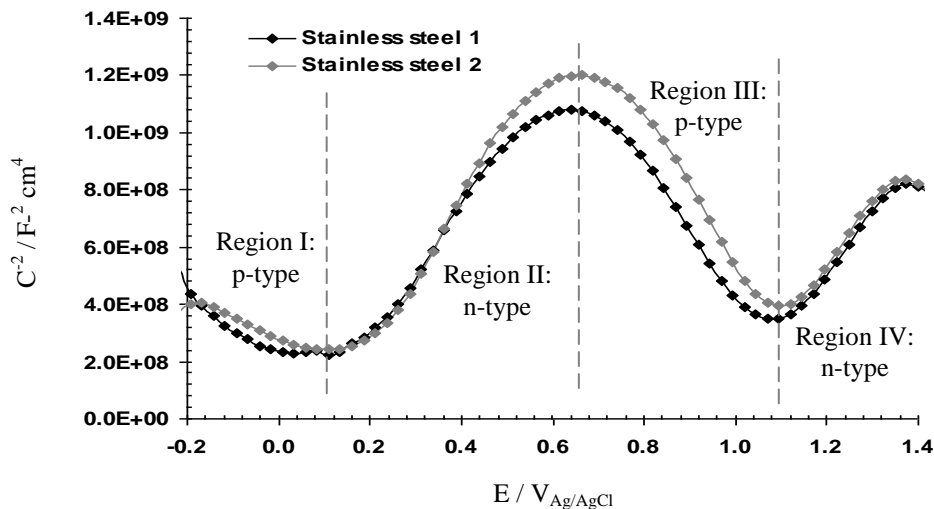


Figure 7: Mott-Schottky plots of two fabricated stainless steels in 0.5M H_2SO_4 solution.

Table 3: Calculated donor and acceptor densities of the passive films formed on two fabricated stainless steels in 0.5M H₂SO₄ solution.

	Donor densities (cm ⁻³)	Acceptor densities (cm ⁻³)
Stainless steel 1	4.225 × 10 ²¹	4.159 × 10 ²¹
Stainless steel 2	3.252 × 10 ²¹	3.171 × 10 ²¹

Changes in donor and acceptor densities correspond to the non-stoichiometry defects in passive films. Therefore, it can be concluded that the passive film on two austenitic stainless steels is disordered. Based on the Point Defect Model (PDM) [29], the donors or acceptors in semiconducting passive layers are point defects. The PDM postulates that the point defects present in a passive film are cation vacancies, oxygen vacancies, and cation interstitials. Cation vacancies are electron acceptors, thereby doping the barrier layer p-type, whereas oxygen vacancies and metal interstitials are electron donors, resulting in n-type doping.

For pure metals, the passive film is essentially a highly doped, defect semiconductor, as demonstrated by Mott-Schottky analysis. Not unexpectedly, the situation with regard to alloys is more complicated than for pure metals; because substitution of other metal cations, having oxidation states different from the host, on the cation sublattice may also impact the electronic defect structure in the film.

Conclusion

The microstructure and electrochemical behaviours of two austenitic stainless steels in 0.5M H₂SO₄ solution were investigated in the present work. Conclusions drawn from the study are as follows

- 1) The amounts of nickel and chromium equivalents and also corrected Schaeffler diagram show that the microstructures of two stainless steels are only austenite. This is also confirmed by optical images and XRD evaluations.
- 2) The potentiodynamic polarization curves show that two fabricated stainless steels showed excellent passive behaviour in 0.5M H₂SO₄ solution
- 3) Mott-Schottky analysis showed existence of a duplex passive film structure composed of two oxide layers of distinct semiconductivities (n-type and p-type).
- 4) Also based on the Mott-Schottky analysis, it was shown that donor and acceptor densities are in the order of 10²¹ cm⁻³ and are comparable for other austenitic stainless steels in acidic environments.

References

1. Kemp M., Van Bennekom A., Robinson FPA. *Mater Sci Eng A*. 199 (1995) 183.
2. Nijhawan BR., in *Stainless Steels '87*. The Institute of Metals, York, (1987).
3. Lula RA., in *Manganese Stainless Steels*. The Manganese Centre, Paris, (1986).
4. Chen SR., Davies HA, Rainforth WM. *Acta mater*. 47 (1999) 4555.
5. Zhang YS., Zhu XM, Zhong SH. *Corros. Sci*. 46 (2004) 853.
6. Bi HY., Jiang XX., Li SZ. *Wear*. 255 (1999) 1043.
7. Lenel UR., Knott BR. *Metall. Trans*. 18 A (1987) 847.
8. Okazaki Y., Miyahara K., Wade N., Hosoi Y. *J. Japan Inst. Metals*. 53 (1989) 502.
9. Masumoto H., Suemune K., Nakajima H., Shimamoto S. *Adv. Cryogenic Engng. Mater*. 30 (1984) 169.
10. Schiller P. *J. Nucl. Mater*. 206 (1993) 113.
11. Miyahara K., Bae DS., Kimura T., Shimoide Y., Hosoi Y. *ISIJ Int*. 37 (1996) 878.
12. Hu B., Kinoshita H., Shibayama T., Takahashi H. *Mater. Trans*. 43 (2002) 622.
13. Harries DR., Butterworth GJ., Hishinuma A., Wiffen FW. *J. Nucl. Mater*. 191 (1992) 92.
14. Kohyama A., Grossbeck ML., Piatti G. *J. Nucl. Mater*. 191 (1992) 37.
15. Shamardin VK., Bulanova TM., Golovanov VN., Neustroyev VS., Povstyanko AV., Ostrovsky ZE. *J. Nucl. Mater*. 233 (1996)162.
16. Onozuka M., Saida T., Hirai S., Kusuhashi M., Sato I., Hatakeyama T. *J. Nucl. Mater*. 255 (1998) 128.
17. Klueh RL., Maziasz PJ., Lee EH. *Mater. Sci. Eng. A*. 102 (1988) 115.
18. Foldefiki M., Ledbetter H., Uggowitz P. *J. Magnetism Magnet. Mater*. 110 (1992) 185.
19. Ruhi G., Modi O.P., Singh I.B. *Corros. Sci*. 51 (2009) 3057.
20. Azumi K., Ohtsuka T., Sata N. *J. Electrochem. Soc*. 134 (1987) 1352.
21. Macdonald D.D., Ismail K.M., Sikora E. *J. Electrochem. Soc*. 145 (1998) 3141.
22. Qiao Y.X., Zheng Y.G., Ke W., Okafor P.C. *Corros. Sci*. 51 (2009) 979.
23. Yang Y., Guo L.J., Liu H. *J. Power Sources*. 195 (2010) 5651.
24. Cheng Y.F., Yang C., Luo J.L. *Thin Solid Films*. 416 (2002) 169.
25. Li N., Li Y., Wang S., Wang F. *Electrochim. Acta*. 52 (2006) 760.

26. Sato N. *Corros. Sci.* 31 (1990)1.
27. Ferreira M.G.S., Hakiki N.E., Goodlet G., Faty S., Simões A.M.P., Da Cunha Belo M. *Electrochim. Acta.* 46 (2001) 3767.
28. Oguzie E.E., Li J., Liu Y., Chen D., Li Y., Yang K., Wang F. *Electrochim. Acta.* 55 (2010) 5028.
29. Macdonald D.D. *J. Electrochem. Soc.* 153 (2006) B213.
30. Fattah-alhosseini A., Golozar M.A., Saatchi A., Raeissi K. *Corros. Sci.* 52 (2010) 205.
31. Fattah-alhosseini A., Soltani F., Shirsalimi F., Ezadi B., Attarzadeh N. *Corros. Sci.* 53 (2011) 3186.

(2014); <http://www.jmaterenvirosci.com>